AIAA 98-3254

PAB3D Simulations of a Nozzle with Fluidic Injection for Yaw Thrust-Vector Control

Karen A. Deere
NASA-Langley Research Center
Hampton, Virginia

34th AIAA/ASME/SAE/ASEE Joint Propulsion Conference & Exhibit
July 13-15, 1998 / Cleveland, OH

PAB3D SIMULATIONS OF A NOZZLE WITH FLUIDIC INJECTION FOR YAW THRUST-VECTOR CONTROL

Karen A. Deere†
NASA Langley Research Center
Hampton, Virginia

ABSTRACT

An experimental and computational study was conducted on an exhaust nozzle with fluidic injection for yaw thrust-vector control. The nozzle concept was tested experimentally in the NASA Langley Jet Exit Test Facility (JETF) at nozzle pressure ratios up to 4 and secondary fluidic injection flow rates up to 15 percent of the primary flow rate. Although many injection-port geometries and two nozzle planforms (symmetric and asymmetric) were tested experimentally, this paper focuses on the computational results of the more successful asymmetric planform with a slot injection port. This nozzle concept was simulated with the Navier-Stokes flow solver, PAB3D, invoking the Shih, Zhu, and Lumley algebraic Reynolds stress turbulence model (ASM) at nozzle pressure ratios (NPRs) of 2, 3, and 4 with secondary to primary injection flow rates (w_s/w_p) of 0, 2, 7 and 10 percent.

INTRODUCTION

Computational fluid dynamic (CFD) methods are often used to complement experimental testing methods for design and analysis of innovative concepts. Numerical simulations can extend an experimental database by providing data for a wide range of flow conditions that would be unrealistic to test in one facility or during the limited term of one test entry. In addition, scaling effects and significant geometric design changes can often be investigated more affordably with CFD simulations.

For certain complex flow fields, the level of accuracy of CFD modeling can vary significantly because of the wide array of flow solvers and turbulence models available. To accurately simulate compressible turbulent flows that will likely include separation and secondary flow structures such as vortices, it is necessary to utilize a Navier-Stokes (N-S) flow solver with an advanced turbulence model. The N-S flow solver, PAB3D, with newly-implemented algebraic Reynolds stress turbulence models (ASM) offers substantial improvement in predicting the peak shear stress of subsonic flow along a flat plate, in determining subsonic and transonic shock wave locations and pressure recovery in separated flow regions along an axisymmetric afterbody, and in simulating the vortices in a supersonic square duct when compared with solutions using a k-ε turbulence model (ref. 1). PAB3D can simulate anisotropies in the flow with ASM by allowing a nonlinear relationship between the stress and velocity gradients which facilitates a more accurate prediction of Reynolds stress differences. The gradients in the Reynolds stresses give rise to secondary flow structures such as the counter-rotating vortices observed in a supersonic square duct. Since the k-ε turbulence model is an eddy viscosity model that relies on a linear relationship between stress and strain, it is difficult to predict complex flow that contains regions of separation and vortices with this type of model.

PAB3D was chosen for the analysis of this convergent exhaust nozzle concept with fluidic thrust vectoring (FTV) because of its ability to accurately predict the internal performance of a variety of nozzle configurations (ref. 2-6). Additionally, an ASM was used to obtain the most accurate simulation of the viscous boundary layer and the turbulent flow developed from the interaction of the multiple flow streams in this application.

FTV uses injection of a secondary air stream into the primary exhaust air stream to cause an off-axis deflection of the primary-jet thrust. The use of fluidics for thrust vectoring can offer significant reductions in exhaust nozzle weight, cost, and complexity by eliminating mechanical moving parts that would otherwise be required for thrust vectoring. Additionally, the lack of moving hardware can result in reduced aircraft observability. Several fluidic thrust vectoring concepts involving the fluidic generation of an oblique shock to turn the primary jet have been

†Aerospace Engineer, Configuration Aerodynamics Branch, Member AIAA

studied with promising results (ref. 7-10). However, these concepts tend to require large injection flow rates and can have significant thrust efficiency penalties resulting from the formation of an oblique shock. The current twin-engine nozzle concept with fluidic injection for yaw thrust-vector control (one nozzle shown in Figure 1) employs sonic-plane reorientation to vector the thrust. Such a concept has the potential for higher thrust efficiency as a result of turning the primary jet at subsonic conditions. The cross-section of the nozzle was designed to facilitate throat realignment between the injection port located at point C and the geometric anchor point located at point A.

This twin-engine nozzle concept was tested experimentally in the NASA Langley Jet Exit Test Facility at nozzle pressure ratios (NPRs) up to 4.0 and secondary fluidic injection flow rates (w_s/w_p) up to 15 percent of the primary flow rate. Although many injection-port geometries and two nozzle planforms (symmetric for a single-engine aircraft and asymmetric for a twin-engine aircraft) were tested experimentally, this paper focuses on the computational results of the more successful asymmetric planform with a slot injection port. This concept was simulated with PAB3D invoking the Shih, Zhu, and Lumley ASM at NPRs of 2, 3, and 4 with secondary fluidic injection flow rates of 0, 2, 7 and 10 percent of the primary flow rate.

NOMENCLATURE

$C_{f,g,sys}$ system resultant thrust coefficient, $\dfrac{F_r}{F_{i,p} + F_{i,s}}$

C_d primary discharge coefficient, $w_p/w_{i,p}$

C_μ turbulence viscosity coefficient, 0.09

F_A measured axial force component, lb

F_N measured normal force component, lb

F_r resultant gross thrust, $\sqrt{F_A^2 + F_N^2 + F_S^2}$, lb

F_S measured side force component, lb

$F_{i,p}$ ideal isentropic thrust of the primary jet, lb

$F_{i,s}$ sum of the ideal isentropic thrust of the secondary injection streams, lb

k turbulent kinetic energy, Pa

N unit normal vector, (n_1, n_2, n_3)

NPR nozzle pressure ratio, $p_{t,j}/p_a$

p local static pressure, psi

p_a ambient pressure, psi

$p_{t,j}$ average jet total pressure, psi

p_∞ free stream static pressure, psi

S_{ij} strain component, 1/sec

U velocity vector

$w_{i,p}$ ideal weight flow rate of primary jet, lb/sec

w_p measured weight flow rate of primary jet, lb/sec

w_s/w_p secondary to primary weight flow ratio

y^+ nondimensional distance of the first grid normal to the surface

δ_y resultant yaw thrust-vector angle, $\tan^{-1}(F_S/F_A)$, degree

ε turbulent energy dissipation

μ laminar viscosity coefficient, m^2/sec

ρ density, slug/ft^3

τ_{ij} Reynolds stress components

EXPERIMENTAL STUDY

Model

The subscale model of the convergent nozzle included a primary duct that transitioned from a rectangular cross-section at the nozzle connect station to a lemon-shaped cross section at the nozzle exit plane. The minimum primary nozzle cross-sectional area was 7.83 in^2 and the ratio of maximum width to maximum height at the nozzle exit when viewed along the nozzle axis was 4.00. The trailing edge of the nozzle was scarfed at a 45 degree angle to aid the yaw thrust-vectoring concept.

Yaw thrust-vector control was accomplished with a secondary air source injecting a stream into the primary duct. The two secondary isolated plenums were located on opposite sides of the nozzle with injection ports opening into the primary duct. The nominal injection-port area was 0.228 in^2 per side. The injection-port geometry was a slot of length 3.5 in. and a width of 0.065 in. that was aligned at a 20 degree angle with respect to a plane perpendicular to the nozzle axis.

Facility Description

The experimental investigation was conducted in the Jet-Exit Test Facility (JETF) at NASA Langley Research Center. This facility is utilized to determine the internal performance of exhaust nozzles at jet-on, static (wind-off) conditions. The JETF test apparatus consisted of a propulsion simulation system, two independently-controllable air supply systems, and a data acquisition system. The primary and secondary air-supply systems were each capable of delivering approximately 23 lb/sec to the test stand although only a fraction of this capability was used for the current test. A complete description of the facility and its capabilities can be found in reference 11.

COMPUTATIONAL STUDY

Governing Equations

The computer code, PAB3D, solves the three-dimensional, Reynolds-averaged Navier-Stokes (RANS) equations and uses one of several turbulence models for closure of the RANS equations. The governing equations are written in generalized coordinates and in conservative form. In an effort to decrease computational resources, the simplified, thin-layer Navier-Stokes equations are implemented into PAB3D. This approximation neglects derivatives in the viscous terms streamwise and parallel to the surface, since they are typically negligible in comparison to the derivatives normal to the surface. Extensive details of PAB3D are found in references 1 and 12.

The flow solver was written with three numerical schemes: the flux vector-splitting scheme of van Leer (ref. 13), the flux difference-splitting scheme of Roe (ref. 14), and a modified Roe scheme primarily used for space marching solutions. These schemes implement the finite volume principle to balance the fluxes across grid cells and the upwind biased scheme of van Leer or Roe to determine fluxes at the cell interfaces. Only the inviscid terms of the flux vectors are split and upwind differenced, while the diffusion terms of the Navier-Stokes equations are centrally differenced. The details and applications of these methods are given in references 12 to 14.

For this study and other typical three-dimensional simulations, the solutions are computed with the van Leer and Roe schemes. An iteration to steady state in a three-dimensional computational domain includes a forward and backward relaxation sweep in the streamwise direction, while implicitly updating each cross plane.

In a two-dimensional computational domain, an index swapping technique is used to speed convergence. Since the cross-plane contains only 1 cell in a two-dimensional computational domain, the streamwise plane is swapped with the cross plane to eliminate the forward and backward relaxation sweep and obtain a fully implicit domain. This procedure typically increases the rate of convergence and decreases the computational space and time required for a converged solution.

Space marching solutions for supersonic flows or subsonic flows with minimal pressure gradients can reduce the computational time necessary for convergence since information travels primarily in one flow direction. Because of the characteristics of supersonic flow, fully implicit solutions may be developed in the streamwise direction by neglecting the upstream information. Implicit solutions are developed by a single forward sweep until the solution converges.

Turbulence Modeling

Turbulence modeling is required to predict solutions for many flow fields. The PAB3D code can perform several turbulence simulations by implementing either an algebraic or 2-equation, linear or nonlinear turbulence model. An algebraic 2-layer, Baldwin-Lomax model is accurate for simple viscous flows because the turbulent viscosity μ_T is determined by a local function. A 2-equation k-ε model with second order closure is used to model more complex viscous flow features. A second equation is used to solve for the turbulent length scale in addition to the equation for turbulent kinetic energy (k). Since the k-ε model has a singularity at solid surfaces, either a damping function or a wall function must be implemented to adjust the turbulent viscosity (ε) near these surfaces. The grid in the boundary layer at wall surfaces must be well defined with a law-of-the-wall coordinate (y^+) of approximately 2 for adequate modeling of the boundary layer flow (ref. 3). The restriction on y^+ may be relaxed to 50 if a wall function is implemented. However, it is customary to restrict the use of wall functions to attached flows.

Both linear and nonlinear turbulence simulations use the standard model coefficients of the k-e equations as a basis of formulation. The linear k-ε turbulence model is an eddy viscosity model with the following formulation for τ:

$$\tau_{ij} = \tau_{ij}^L + \tau_{ij}^T \qquad (1)$$

where,

$$\tau_{ij}^L = \frac{2}{3}\mu_L S_{kk}\delta_{ij} - 2\mu_L S_{ij} \qquad (2)$$

$$\tau_{ij}^T = \frac{2}{3}(\rho k + \mu_T S_{kk})\delta_{ij} - 2\mu_T S_{ij} \qquad (3)$$

$$S_{ij} = \frac{1}{2}\left(\frac{\partial u_i}{\partial x_j} + \frac{\partial u_j}{\partial x_i}\right) \qquad (4)$$

$$\mu_T = f_\mu C_\mu \frac{k^2}{\varepsilon} \qquad (5)$$

The damping function, f_μ, is an empirical function, while C_μ is set to 0.09 for the standard linear k-ε turbulence model. The turbulence model has one equation for turbulent kinetic energy, k, and one for turbulent energy dissipation, ε. This pair of coupled transport equations are written in conservative form

which can be uncoupled from the Navier-Stokes equations and from each other to decrease computational requirements. In an effort to decrease numerical stiffness, the k and ε equations are solved at approximately 25 percent of the Courant-Friedrichs-Levy (CFL) number for the Navier-Stokes equations. Although the linear k-ε turbulence model is widely accepted and utilized in many CFD flow solvers, it inadequately predicts the normal Reynolds-stress differences necessary for predicting anisotropies in the flow. Therefore, to simulate complex flows it is necessary to use an algebraic Reynolds stress model that is able to resolve anisotropic flow features.

Three algebraic Reynolds stress models have been implemented into PAB3D which model a nonlinear relationship between the stresses and velocity gradients; the Shih, Zhu and Lumley (SZL) model, the Gatski and Speziale (GS) model and the Girimaji model. The SZL model (ref. 15) is based on a general turbulent constitutive relation developed by Shih and Lumley in reference 16, which relates the Reynolds stresses to the mean velocity gradients, turbulent kinetic energy, k, and turbulent energy dissipation, ε. The GS model (ref. 17) and the Girimaji model (ref. 18) use an algebraic representation of the pressure-strain correlation illustrated by Speziale et al (ref. 19). However, the GS and Girimaji models each calculate C_μ differently.

Unlike the linear implementation of the standard k-ε equations, the nonlinear implementation requires evaluation of the turbulence stress components at each of the cell faces, instead of at the cell center which is acceptable in the former. Although this increases the number of unknowns per cell, limiting the number of viscous directions that are computed can reduce the number of computed stress components from 36 per cell for a full 3-D grid to 12 or 24 variables per cell.

The Shih, Zhu, Lumley ASM was used in the current simulations of secondary fluidic injection into a primary exhaust flow because of the expectation of separated flow downstream of the injection slot and the secondary flow features arising from the interaction of the primary and secondary flows (normal to the primary flow direction). The PAB3D code was chosen for these simulations because this code was developed for and can accurately predict propulsive flows with mixing, separated flow regions, and jet shear layers. A modified Jones and Launder form (ref. 20) of the damping function (f_μ) was utilized to treat the singularity at the wall. A high Reynolds number model with no damping function was implemented in the free stream blocks.

Performance Calculation

The PAB3D code contains a performance module (ref. 21) that utilizes the momentum theorem applied to a user-defined control volume to calculate nozzle or aerodynamic performance. Quantities such as lift, drag, thrust, moments, heat transfer and skin friction may be computed for many complex geometric configurations and multi-stream flows. Each quantity is updated throughout the solution development to monitor convergence.

Along flow-through sections of the control volume, mass and momentum fluxes, as well as pressure forces are integrated over each cell with equations 6 and 7.

$$w_p = \Sigma\{\rho \boldsymbol{U}\cdot\boldsymbol{N})\,\Delta A \qquad (6)$$

$$\boldsymbol{F}_{flux} = \Sigma\{\rho\boldsymbol{U}\,(\boldsymbol{U}\cdot\boldsymbol{N}) + (p - p_\infty)\boldsymbol{N}\}\Delta A \qquad (7)$$

where ΔA is the cell face area and $\boldsymbol{N}$ is the cell face unit vector.

Along solid surfaces of the control volume, skin friction and pressure forces are determined. Surface pressure force $\boldsymbol{F}_{pressure}$ is determined by multiplying cell static pressure by cell face area using equation 8.

$$\boldsymbol{F}_{pressure} = \Sigma[(p - p_\infty)\boldsymbol{N}]\Delta A \qquad (8)$$

The cell surface static pressure is calculated by extrapolating the cell centered static pressure to the surface where the velocity is assumed to be zero.

The skin friction force $\boldsymbol{F}_{friction}$ is calculated with only the velocity gradients normal to the surface contributing to the velocity terms of the viscous stress tensor. A two point difference is used to determine a velocity gradient, one zero-magnitude velocity vector at the surface and a second at the cell center. Sutherland's formula (ref. 22) is used to calculate the dynamic viscosity at the surface by extrapolating the static temperature at a local cell center to the surface and using a reference viscosity and temperature condition. The total body force vector F is defined in equation 9.

$$\boldsymbol{F} = \boldsymbol{F}_{flux} + \boldsymbol{F}_{pressure} + \boldsymbol{F}_{friction} \qquad (9)$$

Boundary Conditions

The CFD code has many options for defining the conditions of the inflow, outflow, free stream, wall and centerline boundaries. For this study, Riemann invariants along the characteristics were implemented along the lateral and in-flow free stream boundaries. A constant pressure outflow condition was used at the

downstream far field boundary. The nozzle jet and fluidic injection conditions were specified with a fixed total temperature and pressure condition. A no-slip adiabatic wall was implemented to obtain viscous solutions.

Computational Domain

The computational mesh was fully three-dimensional with 7 blocks defining the internal nozzle, 1 block representing the injection plenums and 5 blocks representing the far field domain. The internal nozzle is defined with blocks 1-8 as shown in Figure 2. Block 6, representing the two injection plenums and part of the internal nozzle duct is shown in Figure 3. The i-component is in the x-direction for blocks 1-5 and blocks 7-13 (Figure 2) and in the z-direction for block 6 (Figure 3). Therefore, the principal flow direction follows the i-component for both the primary nozzle stream and the secondary fluidic injection stream. The far field was located 23 throat heights downstream of the nozzle exit, the upper and lower lateral far field was located 17 throat heights above and below the nozzle exit plane. The boundary layer was defined for a law-of-the-wall coordinate y^+ of 0.5 on the fine mesh spacing for adequate modeling of the boundary layer flow.

Grid Study

A grid convergence study was conducted for each predicted solution. Convergence criteria included a two order of magnitude decrease in residual and a variance of less than 0.05 percent in discharge coefficient and 0.1 percent in thrust ratio. Additionally, a grid density (mesh) dependence is established through the comparison of converged performance parameters at several grid levels. Initially, the solution was developed on a coarse mesh which contained one sixteenth the total number of base level (fine mesh) grid points. Once the convergence criteria was met, the solution was interpolated to a medium mesh that included one fourth the total number of base level grid points. Again, the solution was developed until it converged, and finally, the solution was interpolated and converged on the fine mesh. Negligible differences between performance parameters obtained from the medium and fine mesh grids are required to ensure that a solution is independent of mesh density.

Process

Three-dimensional computational solutions were predicted with the Navier-Stokes code, PAB3D, and compared with experimental data at nozzle pressure ratios of 2, 3, and 4 with secondary fluidic injection flow rates of 0, 2, 7 and 10 percent of the primary flow rate. Solutions were computed with near static free-stream conditions.

RESULTS

Comparison of predicted (PAB3D) and experimental (JETF) internal nozzle performance (including discharge coefficient C_d, system resultant thrust ratio $C_{f,g,sys}$, and yaw thrust-vector angle δ_y) with no fluidic injection are shown in Figure 4. There was no separation inside the convergent nozzle which was choked and had a favorable pressure gradient at all three conditions. Therefore, as expected, the correlation between computational and experimental data is excellent. Although these cases had no secondary fluidic injection, the asymmetric geometry of the nozzle produced a non-zero yaw thrust-vector angle. The flow expanded and the throat set up at the geometric minimum area, which was normal to the flow direction (between A and B in Figure 1). Downstream of the throat, the flow was bounded on the inboard side by nozzle hardware, while the jet set up a free shear layer on the unbounded, outboard side. As the flow continued to expand to ambient pressure at the trailing edge, there was an unbalanced side force created from the above ambient pressure acting along the inboard side of the nozzle. To balance this side force, there was a deflection of the primary jet thrust which resulted in a non-zero yaw thrust-vector angle.

Comparison of predicted (PAB3D) and experimental (JETF) internal nozzle performance with 2 percent injection is shown in Figure 5. Discharge coefficient and system resultant thrust coefficient were predicted within 2 percent of experimental data. Predicted yaw thrust-vector angle was predicted within 0.2 degrees at NPRs of 3 and 4. Normalized pressure contours along the nozzle surface (NPR = 4 with w_s/w_p = 0.02) are shown in Figure 6. The flow expanded with a corresponding drop in pressure up to the geometric minimum area. The flow detected a blockage from the fluidic injection and decelerated just upstream of the injection port, which resulted in a region of high pressure. To conserve momentum, an off-axis deflection of the primary jet thrust occurred to balance the asymmetric pressure loading. This resulted in an even larger resultant yaw thrust-vector angle than the no injection case.

The effects of percent of fluidic injection on internal nozzle performance at NPR = 4 are shown in Figure 7. Predicted yaw thrust-vector angle is within 0.3 degrees of experimental data. System resultant

thrust coefficient and discharge coefficient were more difficult to predict at the higher secondary fluidic injection rates, within 2 percent at 7 and 10 percent injection rates.

The no injection solutions were predicted with a computational domain that did include the injection slots and plenums (shown in Figure 2). Although it was necessary to condense the grid around the injection slots to capture relevant features during fluidic injection simulations, the grid bunching near the slots seemed to effect the contours unexpectedly during the no fluidic injection simulations. The sonic lines were aligned with the slots instead of along the geometric minimum area, as expected. To determine if this was a grid effect or a real effect of plenum relief, a second computational domain was generated that did not include the injection slots and plenums.

The effect of modeling the injection slots and plenums on sonic contours and resultant yaw thrust-vector angle, at NPR = 3 with no fluidic injection is shown in Figure 8. The sonic contours are highly curved from the anchor point to the geometric minimum area point when the injection slots and plenums were not modeled (Figure 8(a)). The sonic contours are aligned with the slots and the anchor point when the injection slots and plenums were modeled, which is more closely representative of the experiment (Figure 8(b)). The plenums allowed for relief into the cavity and resulted in a predicted resultant yaw thrust-vector angle well within an expected experimental uncertainty band. The resultant yaw thrust-vector angle was predicted within 0.2 degrees when modeling the internal nozzle geometry without the plenums.

Lessons on Modeling Fluidic Injection

Developing suitable structured grids for complex geometric configurations can be a challenging and iterative process. Modeling secondary air streams, such as fluidic injection for thrust-vector control, can further complicate this process. The current study investigated three methods for modeling the secondary fluidic injection stream. The first and most simple method included a boundary condition at the wall of the primary flow in the location of the injection port. This method proved to be futile for this particular geometry; the flow solver had numerical difficulty at the pinched edge of the nozzle where the boundary conditions, representing the top and the bottom injection ports, met (location C in Figure 1). The second method to model the fluidic injection included a separate grid representation of each injection plenum, each of which had interfaces with a separate primary-flow nozzle block. Again, the flow solver had difficulty at the injection port and primary flow interface planes, even though these interfaces had one-to-one grid matching. The third and successful attempt to model the fluidic injection required a single block representation of both plenums, including the primary flow geometry between the two plenums (Figure 3). This grid topology facilitated a principle flow direction in the i-component for both the injection plenums and the primary-flow nozzle geometry.

CONCLUSIONS

The Navier-Stokes flow solver, PAB3D, was used in a computational investigation of a nozzle, with fluidic injection for yaw thrust-vector control, that was also tested experimentally in the NASA Langley Jet-Exit Test Facility. An algebraic Reynolds stress turbulence model was used to model the turbulent boundary layer and complex flow features associated with this nozzle. The nozzle, which had an asymmetric planform, would be used in a twin-engine aircraft configuration. Solutions were calculated at nozzle pressure ratios of 2, 3, and 4 with secondary fluidic injection flow rates of 0, 2, 7 and 10 percent of the primary flow rate. The results from this investigation indicate the following.

1. PAB3D accurately predicted performance of this complex geometry with no fluidic injection.

2. PAB3D successfully predicted resultant yaw thrust-vector angle within 0.3 degrees at secondary fluidic injection flow rates of 0, 2, 7, and 10 percent of the primary flow rate at a NPR = 4.

3. System resultant thrust coefficient and discharge coefficient were predicted within 2 percent at secondary fluidic injection flow rates of 7 and 10 percent of the primary flow rate.

4. Modeling the injection slots and plenums allowed for a better prediction of yaw thrust-vector angle for the simulations with no fluidic injection.

5. The predicted sonic contour locations were noticeably different when the computational domain included the injection slots and plenums for the simulations with no fluidic injection.

6. Fluidic injection could not be modeled with a boundary condition for this geometry. It was necessary to model the fluidic injection with plenums that included the primary nozzle geometry.

REFERENCES

1. Abdol-Hamid, Khaled, S.: *Implementation of Algebraic Stress Models in a General 3-D Navier-Stokes Method (PAB3D)*. NASA CR-4702, 1995.

2. Abdol-Hamid, Khaled S.; and Pao, S. P.: *Numerical Simulation of Jet Aerodynamics Using the Three-Dimensional Navier-Stokes Code PAB3D*. NASA TP-3596, 1996.

3. Abdol-Hamid, Khaled S.; Lakshmanan, B.; and Carlson, John R.: *Application of Navier-Stokes Code PAB3D With k-ε Turbulence Model to Attached and Separated Flows*. NASA TP-3480, January 1995.

4. Deere, K. A.; and Asbury, S. C.: *An Experimental and Computational Investigation of a Translating Throat Single Expansion-Ramp Nozzle*. AIAA-96-2540, July 1996.

5. Carlson, J. R.; and Reubush, D. E.: *High Reynolds Number Analysis of an Axisymmetric Afterbody with flow Separation*. AIAA-96-2274, June 1996.

6. Carlson, John R.; and Abdol-Hamid, Khaled S.: *Prediction of Static Performance for Single Expansion-Ramp Nozzles*. AIAA-93-2571, June 1993.

7. Wing, David J.: *Static Investigation of Two Fluidic Thrust-Vectoring Concepts on a Two-Dimensional Convergent-Divergent Nozzle*. NASA TM-4574, December 1994.

8. Wing, David J.; and Giuliano, V. J.: *Fluidic Thrust Vectoring of an Axisymmetric Exhaust Nozzle at Static Conditions*. ASME FEDSM97-3228, June 1997.

9. Anderson, C. J.; Giuliano, V. J. and Wing, David J.: *Investigation of Hybrid Fluidic / Mechanical Thrust Vectoring for Fixed-Exit Exhaust Nozzles*. AIAA 97-3148, July 1997.

10. Giuliano, V. J.; and Wing, David J.: *Static Investigation of a Fixed-Aperture Exhaust Nozzle Employing Fluidic Injection for Multiaxis Thrust Vector Control*. AIAA 97-3149, July 1997.

11. A User's Guide to the Langley 16-Foot Transonic Tunnel Complex, Revision 1. NASA TM-102750, September 1990. (Supersedes NASA TM-83186.)

12. Abdol-Hamid, Khaled, S.: *Application of a Multiblock/Multizone Code (PAB3D) for the Three-Dimensional Navier-Stokes Equations*. AIAA-91-2155, June 1991.

13. van Leer, B.: *Flux-Vector Splitting for the Euler Equations*. ICASE Report 82-30, 1982.

14. Roe, P. L.: *Characteristics Based Schemes for the Euler Equations*. A Numerical Review of Fluid Mechanics, 1986, pp. 337-365.

15. Shih, T.-H., Zhu, J., and Lumley, J. L.: *A New Reynolds Stress Algebraic Model*. NASA TM-166644, Inst. for Computational Mechanics, 94-8, 1994.

16. Shih, T.-H., and Lumley, J. L.: *Remarks on Turbulent Constitutive Relations*. NASA TM-106116, May 1993.

17. Gatski, T. B., and Speziale, C. G.: *On Explicit Algebraic Stress Models for Complex Turbulent Flows*. NASA CR-189725, Inst. for Computer Applications in Science and Engineering, 92-58, November 1992.

18. Girimaji, S. S.: *Fully-Explicit and Self-Consistent Algebraic Reynolds Stress Model*. Inst. for Computer Applications in Science and Engineering, 95-82, December 1995.

19. Speziale, C. G., Sarkar, S., and Gatski, T. B.: *Modeling the Pressure-Strain Correlation of Turbulence: An Invariant Dynamical Systems Approach*. Journal of Fluid Mechanics, Vol. 227, 1991, pp. 245-272.

20. Jones, W. P.; and Launder, B. E.: *The Prediction of Laminarization With a Two-Equation Model of Turbulence*. Int. Journal of Heat & Mass Transfer, vol. 15, no. 2, February 1972, pp. 301-314.

21. Carlson, John R.: *A Nozzle Internal Performance Prediction Method*. NASA TP-3221, October 1992.

22. Ames Research Staff: *Equations, Tables, and Charts for Compressible Flow*. NACA Report 1135, 1953.

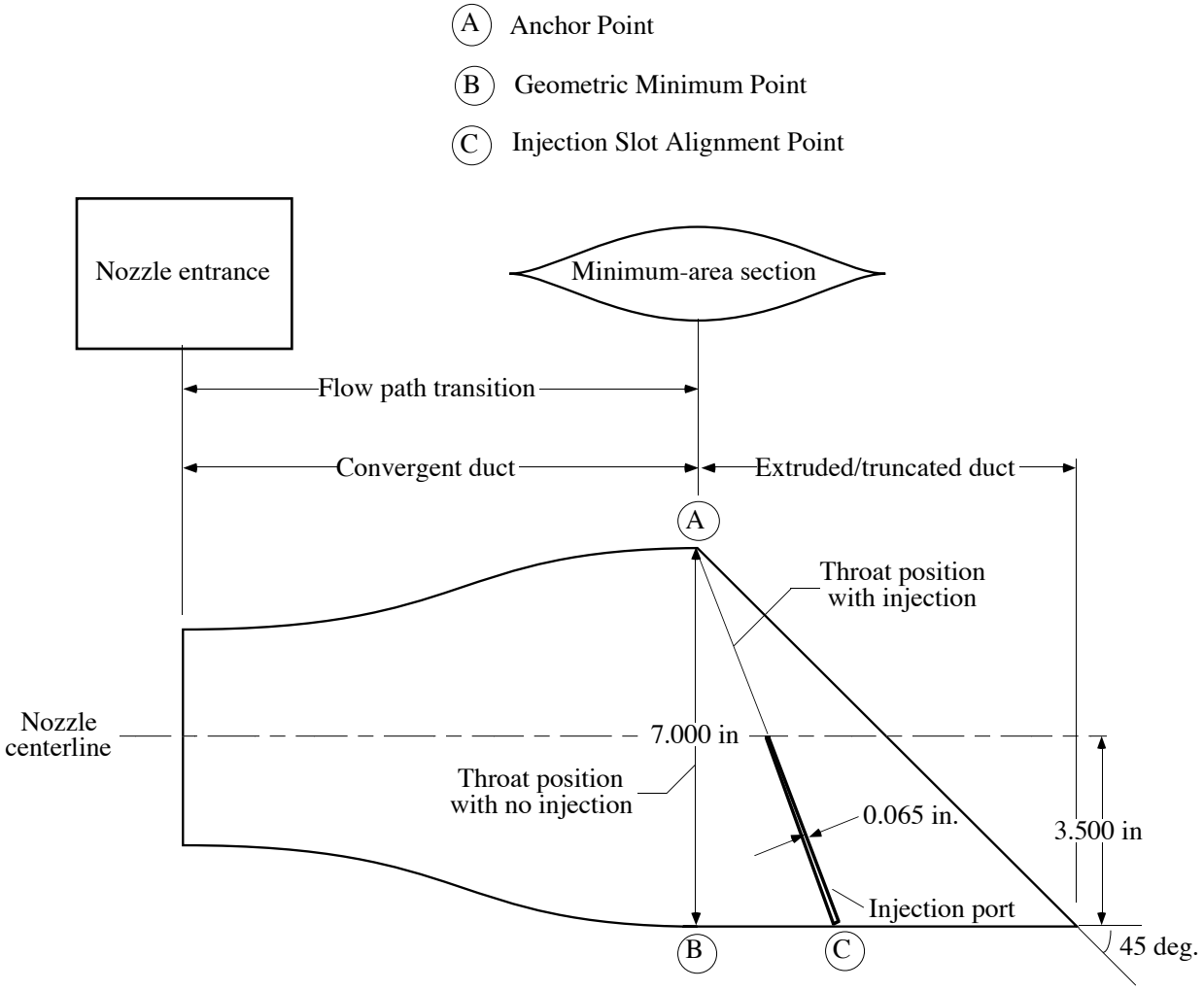

Figure 1. Twin-engine nozzle concept with fluidic injection for yaw thrust-vector control (one nozzle shown).

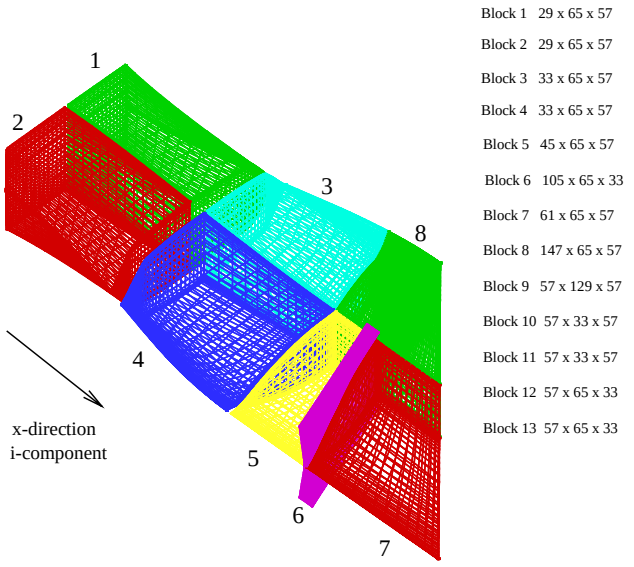

Figure 2. Internal nozzle defined with blocks 1-8.

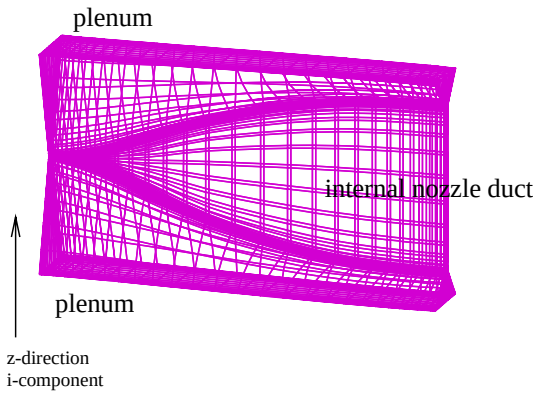

Figure 3. Block 6, representing the injection plenums and internal nozzle duct.

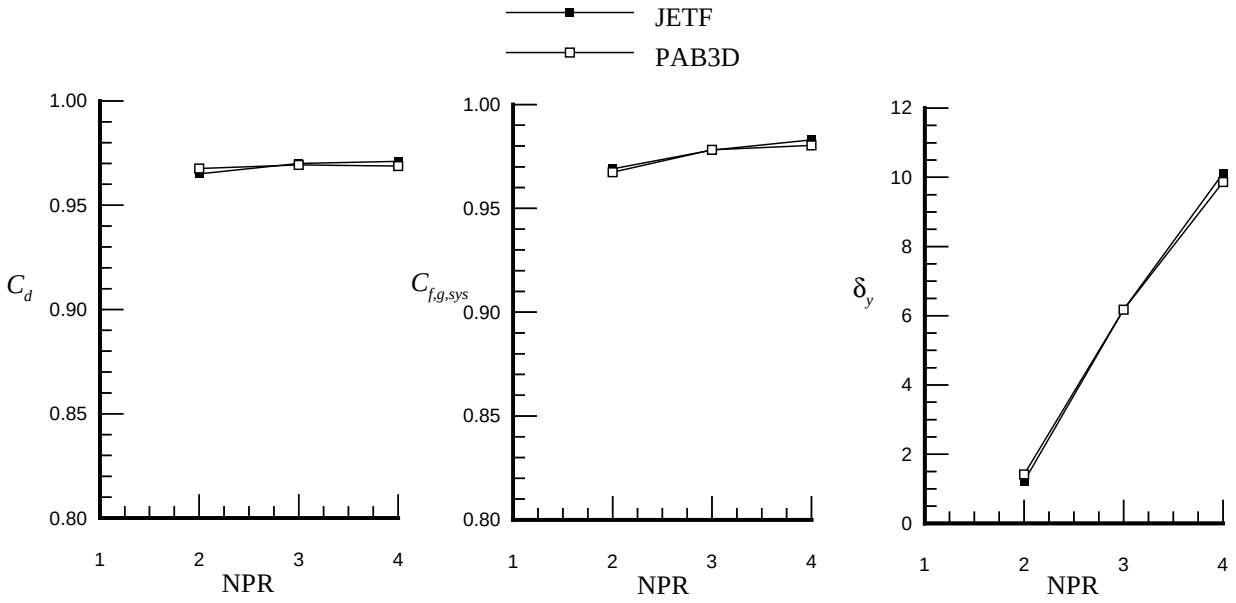

Figure 4. Predicted (PAB3D) and experimental (JETF) internal nozzle performance with no fluidic injection.

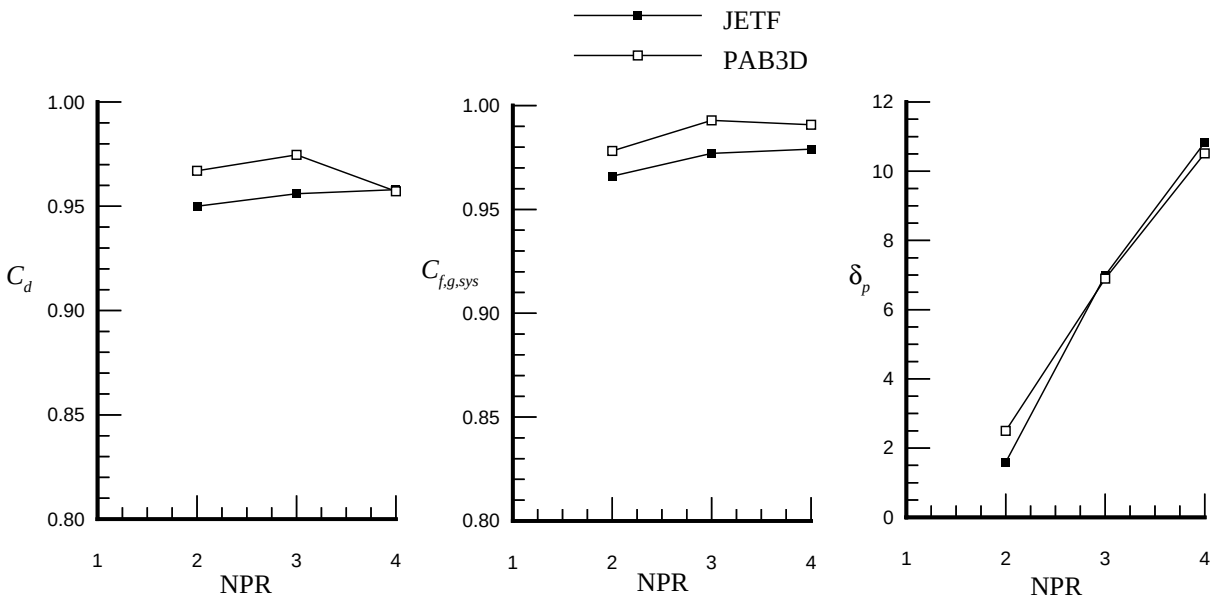

Figure 5. Predicted (PAB3D) and experimental (JETF) internal nozzle performance with 2 percent injection, $w_s/w_p = 0.02$.

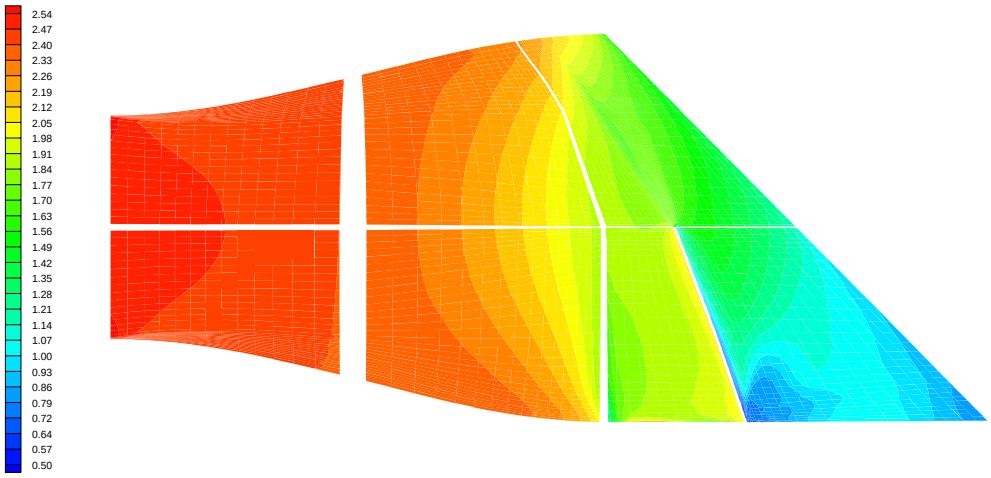

Figure 6. Normalized pressure contours along the nozzle surface, NPR = 4 with $w_s/w_p = 0.02$.

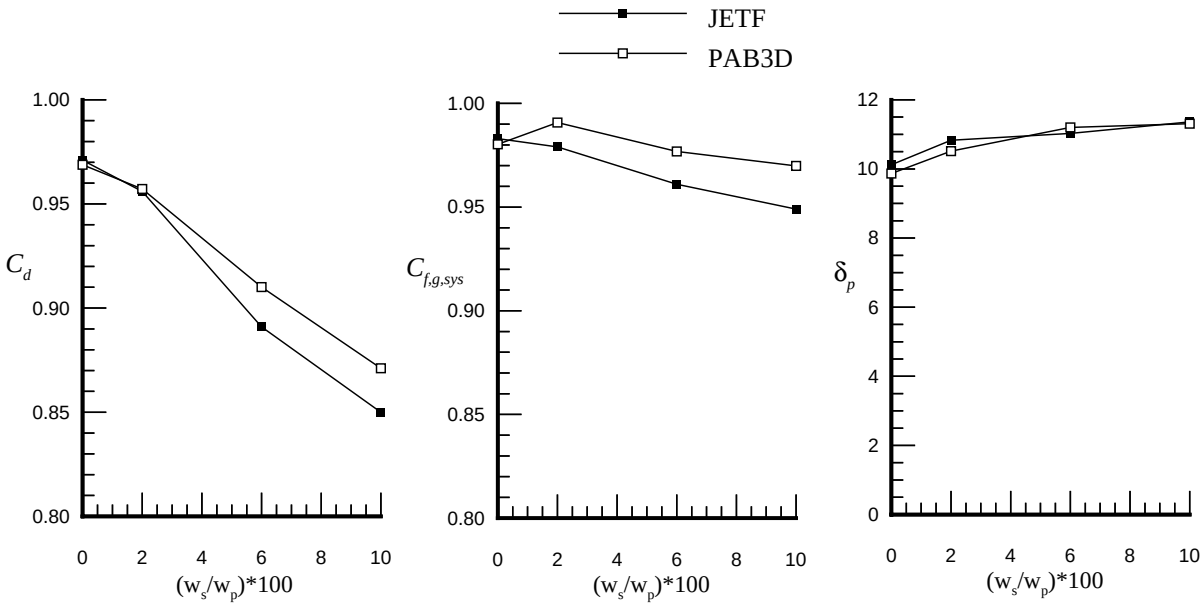

Figure 7. Effects of percent of fluidic injection on internal performance at NPR = 4.

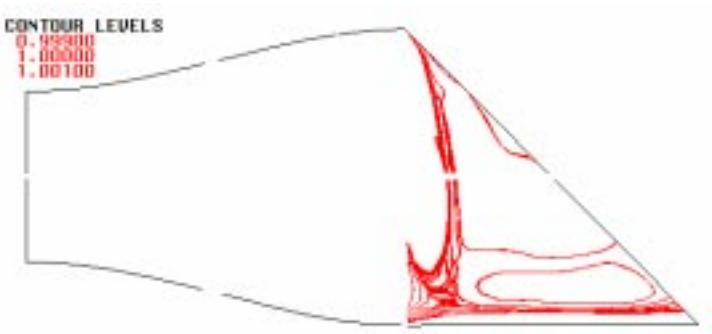

(a) Injection slots and plenums not modeled. $\delta_{y(PAB3D)}$ = 6.025 deg.

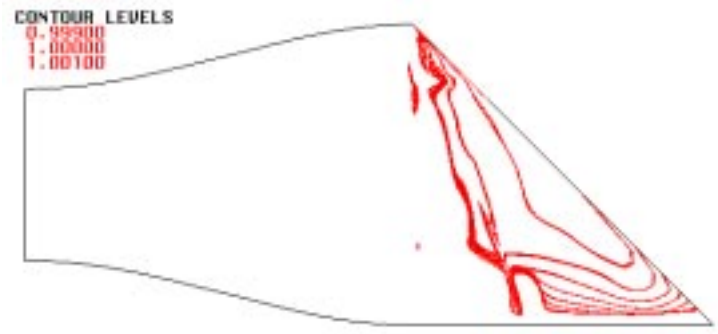

(b) Injection slots and plenums modeled. $\delta_{y(PAB3D)}$ = 6.178 deg.

Figure 8. Effect of modeling injection slots and plenums on sonic contours at NPR = 3 with no fluidic injection, $\delta_{y(JETF)}$ = 6.18 deg.